What's Brought by Micro- and Nanoscopic Approaches to Joining & Welding Metallurgy?†

IKEUCHI, Kenji*

Abstract

Results from TEM (Transmission Electron Microscope) observations made at JWRI are introduced to exemplify nano-scale microstructures that can contribute to improving or controlling the performances of joints produced by fusion welding and solid-state bonding. For fusion welding, the microstructure of a weld metal of 950 MPa class steel was investigated to determine the favorable requirements for both strength and ductility. It is concluded that a mixture of martensite and plate (plus lath) bainite is favorable and the mechanical properties are reduced by the formation of granular bainite, as the hardenability is decreased. For the friction-bonding of Al alloy to steel, it was found that reaction products forming in the interfacial region less than a few μm in width are influenced remarkably by minor alloying elements in the Al alloy, which caused a great difference in the bond strength. With respect to the anodic bonding, by which glass is bonded to metal, by taking advantage of the drift of alkali ions in the glass under an electrostatic field, the debonding phenomenon was investigated by applying an electric field opposite to that applied during bonding. It turned out that the debonding of a glass/Kovar-alloy joint was suppressed by coating the Kovar alloy surface with Al thin film. This effect of the Al coating film is explained as resulting from the properties of interfacial reaction products several 10 nm in size.

KEY WORDS: (transmission electron microscopy), (nano-scale microstructure), (high strength steel), (weld metal), (friction bonding), (aluminum alloy), (steel), (anodic bonding), (glass), (metal),

1. Introduction

Recent advances in the techniques for observation and analysis allow us to reveal the microstructure and distribution of element in materials at the nano-scale. The information about the nano-scale microstructure and element distribution has contributed greatly to the development of advanced materials having excellent properties as well as the scientific understanding of phenomena, through establishing a scientific basis for the improved properties of the materials, enhancing their reliability, improving the productivity, etc.

In the joining and welding field, the contribution of nano-scale information to the practical application in industries will become more important with the progress of the materials to be joined and processes for joining and welding. For example, the weld metal for the high strength steel must be provided with mechanical properties corresponding to the base metal in the as-welded state (as-solidified state) without a heat or mechanical treatment, and to meet the requirements for the strength and ductility, those for more than 800 MPa class steels have very fine microstructure. For this, the weld metal microstructure of these steels is difficult to define by conventional optical microstructure only, and so the favorable microstructure still remains a subject of discussion, leading to a difficulty in alloy design of a weld wire on a scientific basis.

For the solid state bonding and brazing, it has been accepted that the mechanical properties of the joint are in many cases influenced strongly by the interfacial region less than a few μm in width. In these cases, the microstructure of the interfacial region plays a very important role in controlling the joint strength of the solid state bonding and brazing. However, the number of reports about the interfacial microstructure in nano-scale is still limited, probably because of the difficulty of preparing the specimen for the observation.

In this paper, some of our results from TEM (Transmission Electron Microscope) observations of joints produced by fusion welding and solid-state bonding are introduced as examples of nano-scale microstructures that have important effects on joint performances in macro-scale.

† Received on January 31, 2003
* Professor

Transactions of JWRI is published by Joining and Welding Research Institute of Osaka University, Ibaraki, Osaka 567-0047, Japan

2. Microstructure of Weld Metal for 950 MPa Class Steel [1)]

As mentioned in the preceding section, the microstructure of the weld metal for a high strength steel of 950 MPa class is a subject of much discussion, because it is too fine and complicated to identify based on the conventional optical microstructure. Proposed microstructures can be classed into three groups: a mixture of bainite and martensite [2)], acicular ferrite with small amounts of bainite [3)], and a mixture of acicular ferrite and martensite [4)].

Optical microstructures of GMA (Gas Metal Arc) weld metals revealed by Nital etching are shown in **Fig. 1**, for shielding-gas compositions of pure Ar, Ar + 10% CO_2, and Ar + 25% CO_2. When the shielding gas was pure Ar, the weld metal microstructure consisted mainly of a very fine lath structure. The lath structure was coarsened and degraded gradually with the addition of CO_2 to the shielding gas, while granular structure became more dominant as shown in Figs. 1(b) and 1(c). The addition of CO_2 to the shielding gas had also strong influences on the hardness value and the Charpy energy as shown in **Fig. 2**, suggesting that the microstructural change shown in Fig. 1 contributed significantly to the reduction in the hardness and ductility with the CO_2 addition.

Microstructures observed with a TEM are shown in **Figs. 3-5**. When the shielding gas was pure Ar, as shown in **Fig. 3**, a lath structure much finer than those observed using optical microscope was observed. The individual lath had a high dislocation density, and was identified as BCC (BCT) based on the SAD pattern. Between some of these laths, a second phase was observed which was identified as retained austenite. When the CO_2 content of the shielding gas was 10%, the lath structure was coarsened in comparison with those observed when the shielding gas was pure Ar, but it was still a dominant microstructure (see **Fig. 4**). The second phase observed between the laths was also identified as retained austenite. When the CO_2 content of the shielding gas was increased to 25%, as shown in **Fig. 5**, the microstructure consisted of a non-lath structure and lath structure similar to those observed at a CO_2 content of 10%. In the non-lath structure, M-A constituents were observed. TEM micrographs of a M-A constituent observed in the non-lath structure are shown in **Fig. 6**. The SAD pattern and dark field image shown in Figs. 6(b) and 6(c) show that the peripheral area of the dark island observed in the bright field image (Fig. 6(a)) consisted of retained austenite. Those shown in Figs. 6(d)-6(g) indicate that the internal area surrounded by the retained austenite consisted of twinned martensite, viz., high carbon martensite. These results show obviously that the dark island shown in Figs. 6(a) and 6(d) is an M-A constituent.

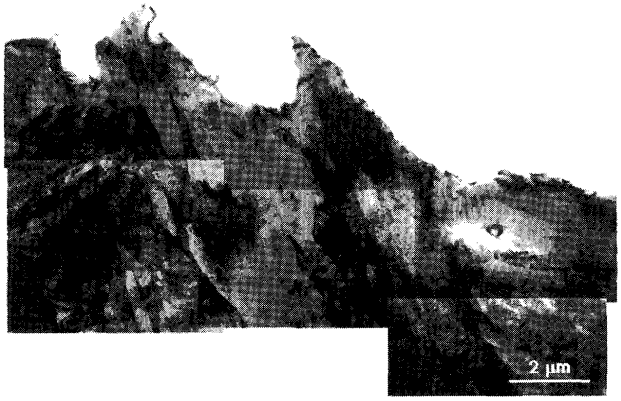

Fig. 3 TEM micrograph of a GMA weld metal using shielding gas of pure Ar.

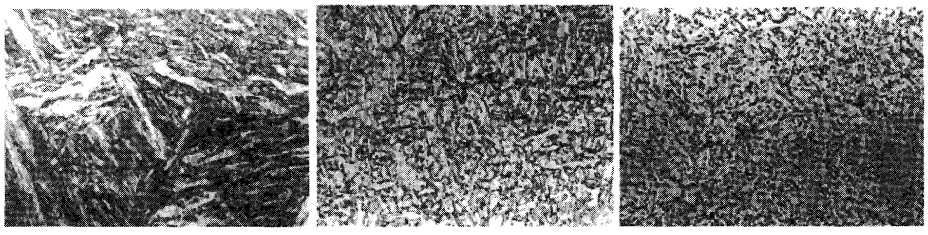

Fig. 1 Optical microstructure of GMA weld metal for 950 MPa class steel.

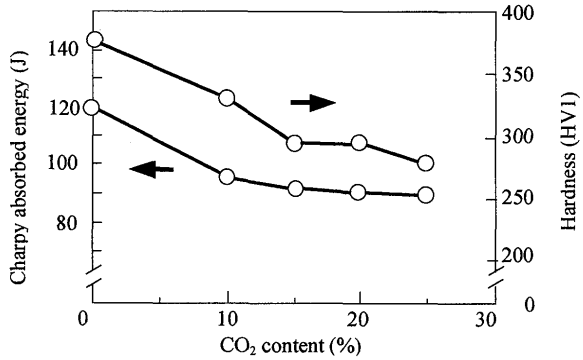

Fig. 2 Effects of CO_2 content of the shielding gas on Charpy absorbed energy and hardness of GMA weld metals.

It has been said that the bainite formed in the HSLA steel through continuous cooling transformation can be classified into two types, depending on the cooling rate. The bainite formed at slower cooling rates is characterized by its granular morphology (at optical-microscopy scale) and the formation of the M-A constituent. The mechanical properties of the granular bainite are inferior to those of the plate or lath bainite formed at faster cooling rates. The superior mechanical properties observed at lower CO_2 contents of the shielding gas and observed features of the microstructures indicate that the weld metal for the 950 MPa class steel consisted primarily of martensite and bainite, and the amount of granular bainite increased with the CO_2

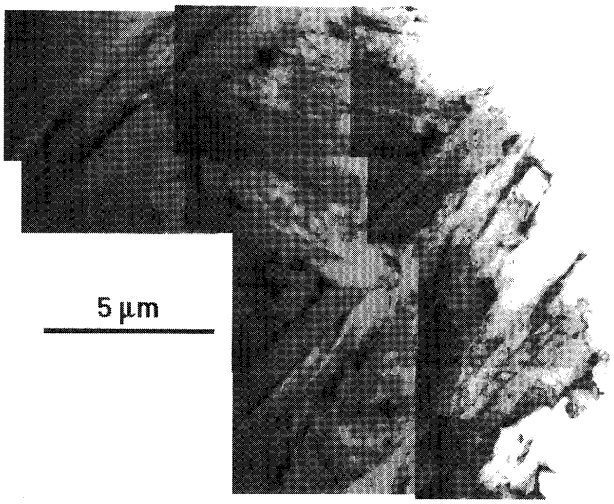

Fig. 4 TEM micrograph of a GMA weld metal using shielding gas of Ar+10%CO_2.

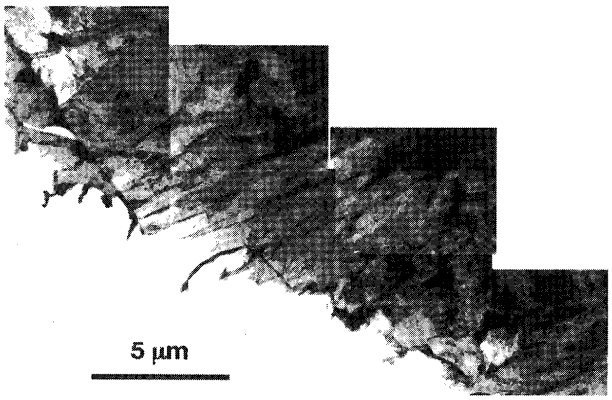

Fig. 5 TEM micrograph of a GMA weld metal using shielding gas of Ar+25%CO_2.

addition to the shielding gas at the expense of the other microstructures.

3. Effect of Alloying Element on Microstructure and Bond Strength of Friction-Bonded Interface of Al Alloy to Steel

Friction bonding has been widely applied to the joining of dissimilar metals, since the interfacial reaction that often forms brittle intermetallic compounds can be controlled through a suitable choice of bonding parameters. In particular, many investigations have been reported of the friction bonding of Al alloy to steel. Several authors [5] have suggested that the bond strength not less than the base-metal strength is rather difficult to obtain even by friction bonding, depending on the chemical composition of the Al alloy. The reason for this, however, still remains unclear for the lack of the information about the microstructure of the interfacial region.

For example, the bond strength and joint efficiency estimated from tensile strength of a specimen with a circumferential U-notch at the interface are shown in **Fig. 7**, for joints of a S10C mild steel specimen to a 5052, 5083, or 6061 Al-alloy specimen. The joint efficiency depended significantly on the chemical composition of the Al alloy, although the joints were bonded under the same conditions. SEM observations revealed that an intermetallic compound layer was formed at the interface of these joints as shown in **Fig. 8**. It has been said that the harmful effect of the brittle intermetallic compound layer on the bond strength becomes more serious, as its thickness is increased [6]. However, the S10C/5083 joint that showed the lowest bond strength had the narrowest intermetallic compound layer, and the intermetallic compound layer observed in the S10C/6061 joint was narrower than that observed in the S10C/5052 joint, whereas the joint efficiency of the S10C/6061 joint was

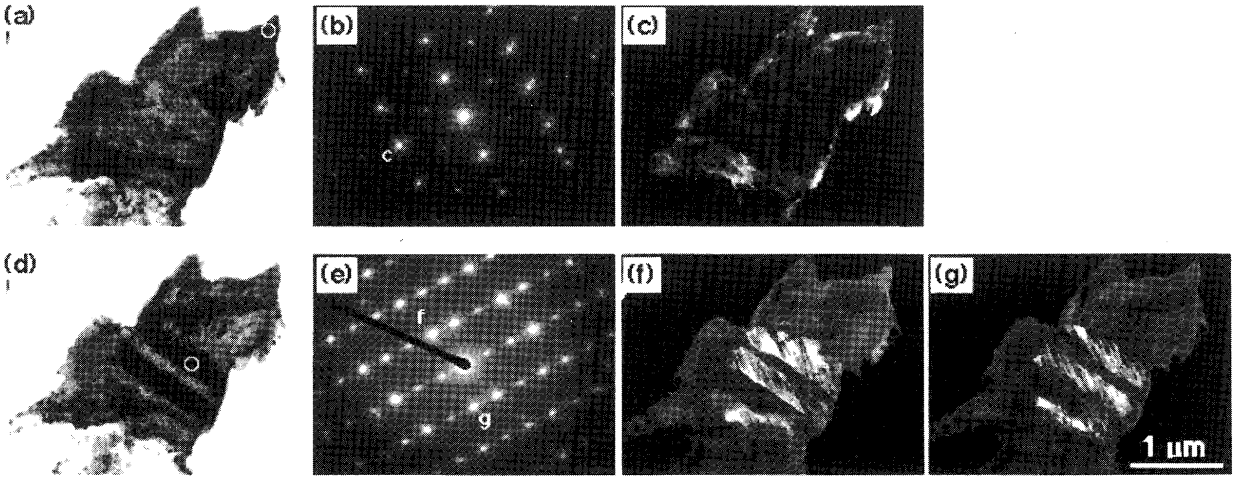

Fig. 6 TEM micrographs of an M-A constituent observed in a weld metal using a shielding gas of Ar+25%CO_2: (a) Bright field image, (b) SAD pattern from retained austenite, (c) dark field image of retained austenite, (d) bright field image observed from a different direction, (e) SAD pattern from twinned martensite, (f) dark field image of twinned martensite, and (g) dark field image of twinned martensite.

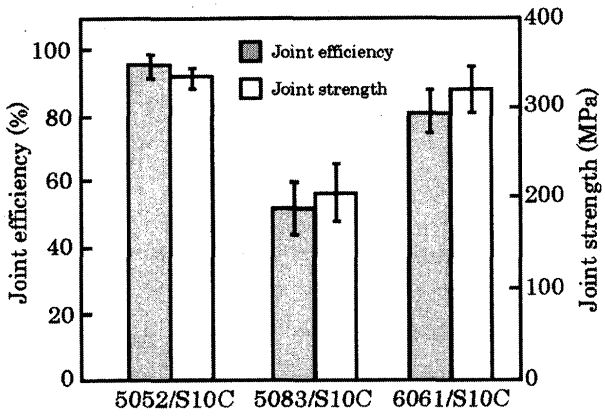

Fig. 7 Joint efficiency and strength of friction-bonded joints of a mild steel S10C specimen to an Al alloy specimen 5052, 5083, or 6061. The joint efficiency A is given by A = (tensile strength of joint) / (tensile strength of the Al base metal specimen with the same dimensions).

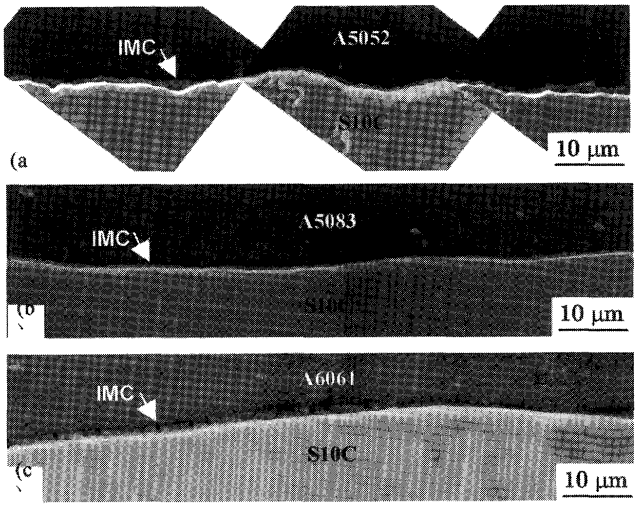

Fig. 8 SEM micrographs of S10C/5052 (a), S10C/5083 (b), and S10C/6061 joints (c), where IMC indicates intermetallic compound layer.

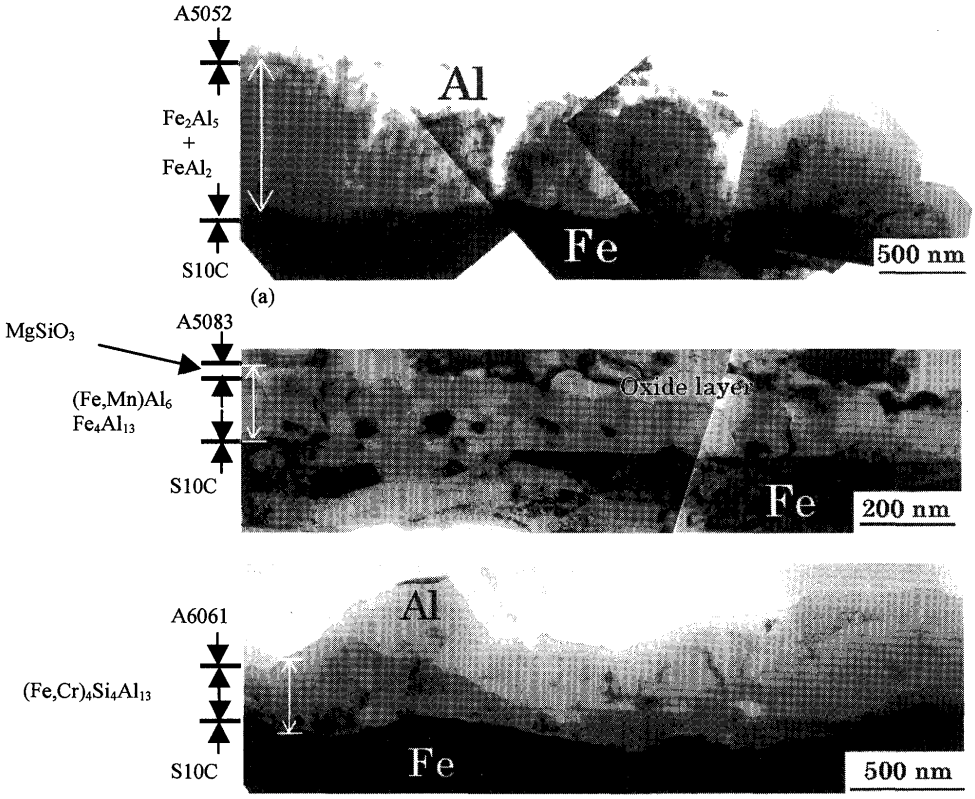

Fig. 9 TEM micrographs of S10C/5052 (a), S10C/5083 (b), and S10C/6061 joints (c).

lower. These results suggest that the intermetallic compound layer formed at the friction-bonded interface of steel to Al-alloy consisted of different phases depending on the chemical composition of the Al alloy.

Therefore, the TEM observations of the intermetallic compound layers have been carried out to identify the comprised phases. The TEM micrographs of S10C/5052, S10C/5083, and S10C/6061 interfaces are shown in **Fig. 9**. The interfacial reaction layers consisted of a mixture of Al_2Fe and Al_5Fe_2 grains for the S10C/5052 joint, Fe_3Al_4, $Al_6(Mn,Fe)$, and $MgSiO_3$ layers for the S10C/5083 joint, and $(Fe,Cr)_4Si_4Al_{13}$ layer for the S10C/6061 joint. These results indicate that the minor alloying elements like Mn and Si (see **Table 1**) can have

Table 1 Chemical compositions of the Al alloys employed (mass%).

Alloys	Si	Mn	Cu	Cr	Mg	Zn	Ti	Fe	Al
5052	0.07	0.01	0.01	0.26	2.60	0.01	-	0.21	Bal.
5083	0.22	0.60	0.07	0.11	4.70	0.01	-	0.21	Bal.
6061	0.50	-	0.32	0.06	1.00	0.01	0.01	0.23	Bal.

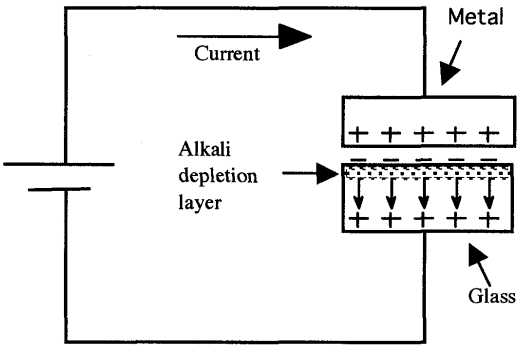

Fig. 10 Schematic illustration of anodic bonding.

strong influence on the kind of intermetallic compounds formed during the friction bonding. In other words, this suggests that the intermetallic compound layer formed at the friction-bonded interface can be controlled by adjusting the content of minor alloying elements to improve the bond strength.

4. Microstructure of Anodically-Bonded Interface and Debondability

Anodic bonding is a process to join glass to metal by applying an electrostatic field at a temperature (550 - 600 K) high enough for alkali cations in the glass to have long-range mobility. As shown in **Fig. 10**, negative charges due to the formation of excessive oxygen anions are accumulated in the surface layer of the glass as a result of the migration of alkali cations toward the cathode side, and they exert an electrostatic attractive force to the metal to bring the metal and glass surfaces into intimate contact. In addition, the excessive oxygen anion formed in the glass reacts with the metal surface to form an oxide layer that acts as a binder between the glass and metal. Anodic bonding is widely applied as a sealing process for electronic sensors and as an assembling process for electronic devices, since it enables bonding at lower temperatures than the glass softening-point without significant residual strain.

A salient feature of this process, we think, is that the direction of electric field, a bonding parameter, can be reversed. In **Fig. 11** is shown the effect of the reversed electric field (in the opposite direction to that applied during bonding) on the contacted area of anodically-bonded joints. The joints employed were those of borosilicate glass to Kovar alloy and borosilicate glass to Al film deposited on Kovar alloy surface. The contacted areas were almost 100% in the as-bonded state for both joints. As the application time of the opposite electric field was increased, as shown in Fig. 11, the contact area of the glass/Kovar joint decreased rapidly, and finally the joint was debonded. In contrast, the opposite electric field had almost no influence on the contacted area, when the Kovar alloy surface was coated with the Al film.

Thus, the effect of the opposite electric field on the contacted area of the glass/Kovar interface was completely changed by coating the Kovar alloy surface with the Al thin film. In order to explain such completely different behaviors under the opposite electric field, the

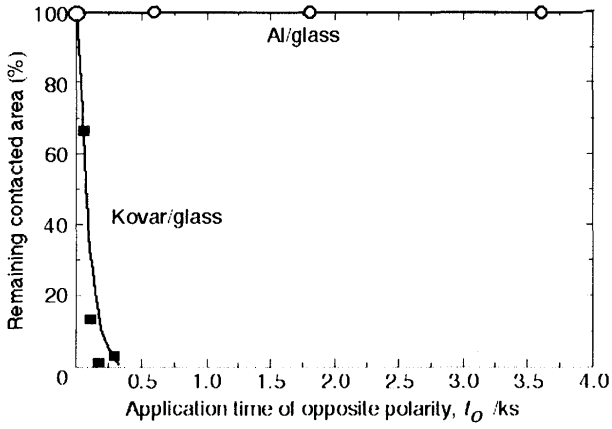

Fig. 11 Effect of opposite electric field on the contacted areas in joints of glass to Kovar alloy and of glass to Al-coated Kovar alloy.

bond interface was observed with a TEM. As shown in

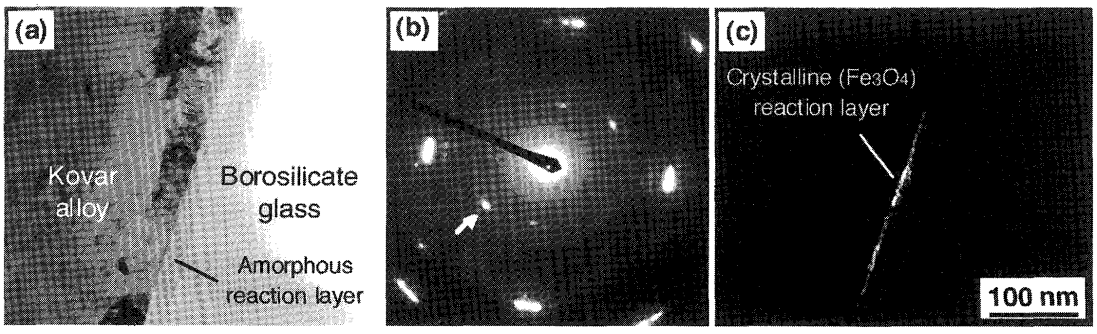

Fig. 12 TEM micrographs of an anodically bonded joint of a borosilicate glass to Kovar alloy: (a) bright field image, (b) SAD pattern, and (c) dark field image of Fe_3O_4 layer.

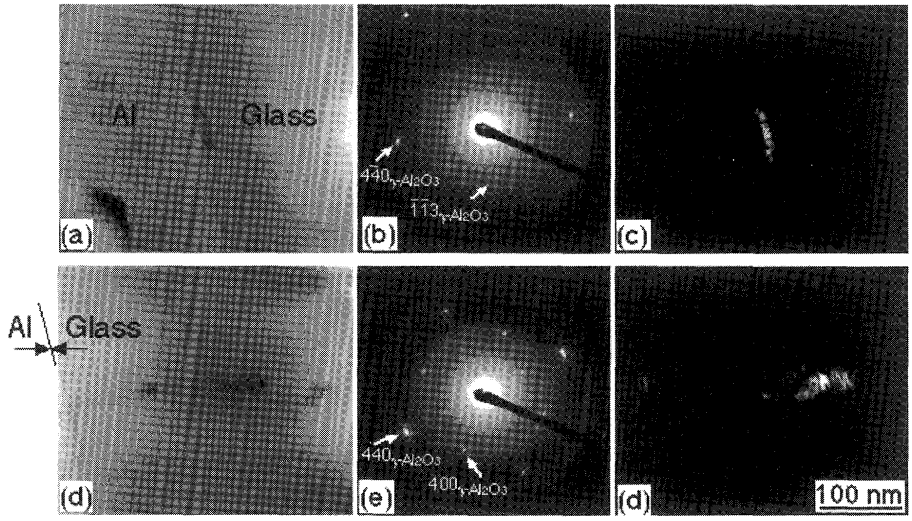

Fig. 13 TEM micrographs of a anodically bonded joint of borosilicate glass to Al-coated Kovar alloy. (a), (b), (c) are bright field image, SDA pattern and dark field image of a γ-Al_2O_3 layer, respectively. (d), (e), and (f) are those of fibrous γ-Al_2O_3 crystal.

Fig. 12, an amorphous layer of Fe-Si oxide a few 10 nm in width and crystalline oxide layer of Fe_3O_4 ~10 nm in width were found at the glass/Kovar interface. On the other hand, crystalline layers of γ-Al_2O_3 and fibrous γ-Al_2O_3 were formed at the interface of glass to Al film (see **Fig. 13**). Thus the morphology of the interfacial reaction products was completely different between the glass/Kovar and glass/Al interfaces. It can be expected that the fibrous oxide observed at the glass/Al interface contributes to reinforcing the bond interface by so-called anchoring effect, and avoids the localized concentration of Na at the interface under the opposite electric field (considered to be the cause for the debonding phenomenon).

Durability to the opposite electric field is an important property for the fabrication of a layered structure consisting of two conducting plates (metal or semiconductor) separated by an insulating spacer (glass). On the other hand, the debonding phenomenon can be used for the fractional recovery of the bonded materials from a disposed joint for recycling. Thus two completely different properties can be given to the glass/metal joint through controlling the microstructure of the interface in nano-scale.

5. Conclusions

Some of our results from TEM observations made at JWRI are introduced. It should be emphasized that the observed microstructures are present in the joints to be practically used in industrial structures and contribute to maintaining the required performances of the whole structures as well as the joint itself. There should be similar cases other than these where the nano-scale microstructure plays an important role in controlling the joint performances.

Of course, careful discussion to understand the formation process and mechanism of the microstructure, and to explain how the microstructure is correlated with joint performances is indispensable for improving and controlling the joint performances. For this discussion, however, the observation for clear identification of the microstructure is essential, considering that the formed microstructure is difficult to predict, probably because of the non-steady state and/or non-equilibrium characteristics of the joining and welding processes as suggested by those observed at the interfaces of friction bonding (see Fig. 9) and anodic bonding (see Figs. 12 and 13).

Needless to say, the information about the nano-scale microstructure and element distribution will become increasingly important with the rapid progresses made in the fields of electronic devices, micromachining, and nano-technology, where the extensive applications of joining and welding can be expected.

References

1) M.A. Gouda, M. Takahashi, T. Kuroda, and K. Ikeuchi: Sci. Tech. Weld. Join., to be published.
2) N.A. Fleck, O. Grong, G.R. Edwards, and D.K. Matlock: Weld. J., **15**(1986), 113-s.
3) Z. Yang and T. Debroy: Metall. Trans. B, **30B**(1999), 483.
4) J.E. Ramirez, S. Liu, and D.L. Olson: Mater. Sci. Eng., A216(1996), 91.
5) H. Ochi, K. Ogawa, Y. Yamamoto, S. Hashinaga, and Y. Suga: J. Japan Inst. Light Metals, **46**(1996), 500.
6) T. Enjo, K. Ikeuchi, and N. Akikawa: J. Japan Weld. Soc., **48**(1979), 770.